Progress of Theoretical Physics, Vol. 107, No. 2, February 2002

Effect of Parameter Mismatch and Noise on Weak Synchronization

Sang-Yoon Kim,[1] Woochang Lim[1] and Youngtae Kim[2]

[1]*Department of Physics, Kangwon National University, Chunchon, Kangwon-Do 200-701, Korea*
[2]*Department of Molecular Science and Technology, Ajou University, Suwon, Kyunggi-Do 442-701, Korea*

(Received October 29, 2001)

We have numerically investigated the effect of parameter mismatch and noise on the loss of chaos synchronization in unidirectionally coupled one-dimensional maps. Through a first transverse bifurcation of an unstable periodic orbit embedded in the synchronous chaotic attractor (SCA), this attractor becomes weakly stable. In the regime of weak synchronization, any small parameter mismatch and noise transform the SCA into a bubbling attractor or a chaotic transient. In this case, the quantities of interest are the average interburst interval of the bubbling attractor and the average lifetime of the chaotic transient. They are found to scale with the mismatching parameter and the noise intensity. Furthermore, the scaling results for the cases of parameter mismatch and noise are quantitatively the same. We also give the theoretical background for the scaling by comparing our numerical results with theoretical results. For the bubbling case, the maximum bursting amplitude is another quantity of interest. We discuss the abrupt increase in the maximum bursting amplitude that results from the sudden increase in the size of the absorbing area, confining the bursting, through an interior crisis. This is in contrast with the case of symmetric coupling, in which no such crisis occurs for the absorbing area.

§1. Introduction

Many dynamical systems of interest have an invariant subspace embedded in the whole phase space. For example, this situation occurs naturally in the synchronization of chaotic oscillators.[1)-4)] Particularly, this chaotic synchronization has attracted much attention, because of its potential practical application to secure communication.[5)]

If a synchronous chaotic attractor (SCA) on the invariant subspace is stable with respect to perturbations transverse to the invariant subspace, then it may become an attractor in the whole phase space. Such a transverse stability of the SCA is intimately associated with transverse bifurcations of unstable periodic orbits embedded in the SCA.[6)-12)] If all such unstable periodic orbits are transversely stable, the SCA becomes asymptotically stable, and hence we have "strong" synchronization. However, as the coupling parameter passes through a threshold value, a periodic saddle first becomes transversely unstable through a local bifurcation. After this first transverse bifurcation, trajectories may be locally repelled from the invariant subspace when they visit the neighborhoods of the transversely unstable periodic orbit points and their preimages. Thus, loss of strong synchronization begins with such a first transverse bifurcation, and as a result we have "weak" synchronization. Therefore, a typical trajectory on the weakly stable SCA may have segments exhibiting positive

local Lyapunov exponents, even if the average transverse Lyapunov exponent is negative. For this case, intermittent bursting or basin riddling may occur, depending on the existence of an absorbing area, controlling the global dynamics, inside the basin of attraction.[10)-13)] In the presence of an absorbing area, acting as a bounded trapping vessel, locally repelled trajectories from the invariant subspace are restricted to move within the absorbing area, and exhibit transient intermittent bursting from the invariant subspace.[14),15)] By constrast, in the absence of such an absorbing area, locally repelled trajectories will go to another attractor (or infinity), and hence the basin of attraction becomes riddled with a dense set of repelling "holes", belonging to the basin of another attractor (or infinity).[16)]

However, in a real situation, a small mismatch between the subsystems that destroys the invariant subspace and noise are unavoidable. To understand such a situation, we numerically investigated the effect of parameter mismatch and noise on the bursting and basin riddling in two unidirectionally coupled one-dimensional (1D) maps with an invariant diagonal. For the case of bursting, any small parameter mismatching and noise results in a continual sequence of intermittent bursts, called attractor bubbling, where the long period of nearly synchronous states (laminar phase) is randomly interrupted by short-time bursts (burst phase). For the case of riddling, the SCA on the diagonal is transformed into a chaotic transient. In both cases, the quantity of interest is the average time τ that a trajectory spends near the diagonal (i.e., the average interburst interval and the average lifetime of the chaotic transient).[15)] We investigate how τ scales with the mismatch parameter ε and the noise intensity δ in §2. Near the first transverse bifurcation point, τ increases faster than any power of ε^{-1} or δ^{-1} as ε or δ goes to zero. However, after passing a crossover region, τ exhibits a power-law scaling. As c approaches the blow-out bifurcation point, where the transverse Lyapunov exponent becomes zero, the scaling exponents decrease because τ becomes shorter. After the blow-out bifurcation, the weakly stable SCA becomes transversely unstable.[17)] Note that in both cases of parameter mismatch and noise, the scaling exponents are the same. Thus the scaling results for the cases of parameter mismatch and noise on τ become quantitatively the same. We also give the theoretical background for the superpower-law and power-law scalings by comparing our numerical results with theoretical results. In §3, we investigate the change in the maximum bursting amplitude for the attractor bubbling by varying the coupling parameter. At first, the maximum bursting amplitude begins to increase smoothly. However, when passing a threshold value, it increases abruptly, due to the sudden increase in the size of the absorbing area, confining the bursting, through an interior crisis. This is in contrast to the symmetric-coupling case, in which no such crisis of the absorbing area occurs. Finally, we give a summary in §4.

§2. Average interburst interval and average lifetime of the chaotic transient

We investigate the effect of parameter mismatch and noise on weak synchronization in unidirectionally coupled 1D maps[11)] defined by

$$T : \begin{cases} x_{n+1} = f(x_n, a) + \delta\, \xi_n^{(1)}, \\ y_{n+1} = f(y_n, b) + c\, g(y_n, x_n) + \delta\, \xi_n^{(2)}, \end{cases} \tag{1}$$

where x_n and y_n are state variables of the subsystems at the discrete time n. The local dynamics in each subsystem with the control parameter p ($p = a, b$) is governed by the 1D map $f(x, p) = 1 - p\,x^2$, c is the coupling parameter between the two subsystems, and $g(x, y)$ is a coupling function of the form

$$g(x, y) = y^2 - x^2. \tag{2}$$

Note that the first master 1D map can be regarded as a driving for the second slave or response 1D map. For the case of identical 1D maps (i.e., $a = b$), there exists an invariant synchronization line, $y = x$, in the $x - y$ phase space. However, in the presence of a mismatching between the two 1D maps, the diagonal is no longer invariant. To take into consideration such a mismatching effect, we introduce a small mismatching parameter ε in the coupled 1D maps of Eq. (1) such that

$$b = a - \varepsilon. \tag{3}$$

Furthermore, noise is unavoidable in a real situation. Hence, an additive random noise is considered in Eq. (1). For this case, $\xi_n^{(1)}$ and $\xi_n^{(2)}$ are independent random numbers chosen from a uniform distribution with zero mean ($\langle \xi_n \rangle = 0$) and unit variance ($\langle \xi_n^2 \rangle = 1$), and δ controls the "strength" of such a random noise.

For the noiseless case with $\delta = 0$, the unidirectionally coupled map T is non-invertible, because its Jacobian determinant $\det(DT)$ (where DT is the Jacobian matrix of T) becomes zero along the critical curves, $L_0 = \{(x, y) \in R^2 : x = 0 \text{ or } y = 0\}$. The critical curves of rank k, L_k ($k = 1, 2, \ldots$), are then given by the images of rank k of L_0 [i.e., $L_k = T^k(L_0)$]. Segments of these critical curves can be used to define a bounded trapping region in the phase plane, called an 'absorbing area $\mathcal{A}$,' with the properties that (i) trajectories that enter $\mathcal{A}$ cannot leave it again, and (ii) there exists a neighborhood $U \supset \mathcal{A}$ whose points enter $\mathcal{A}$ in a finite number of iterations.[13] Furthermore, boundaries of an absorbing area can also be obtained by the union of segments of critical curves and portions of unstable manifolds of unstable periodic orbits. For this case, $\mathcal{A}$ is called a 'mixed absorbing area'. Note that the fate of locally repelled trajectories from the diagonal depends on the existence of such an absorbing area $\mathcal{A}$. In presence of $\mathcal{A}$, they are confined to move within $\mathcal{A}$, while in absence of $\mathcal{A}$, they go to another attractor. In this way, the absorbing area $\mathcal{A}$ controls the global dynamics.

As an example, we consider the SCA that exists in the interval $c_{b,l}\,(\simeq -2.963) < c < c_{b,r}\,(\simeq -0.677)$ for $a = 1.82$ when $\varepsilon = \delta = 0$. As the coupling parameter c passes through $c_{b,l}$ or $c_{b,r}$, the SCA becomes transversely unstable through a blow-out bifurcation, and then a complete desynchronization occurs. In the regime of synchronization, a strongly stable SCA exists for $c_{t,l}\,(= -2.789\,372) < c < c_{t,r}\,(= -0.850\,625)$, because all periodic saddles embedded in the SCA are transversely stable. However, when the coupling parameter c passes through $c_{t,r}$ and $c_{t,l}$, bubbling

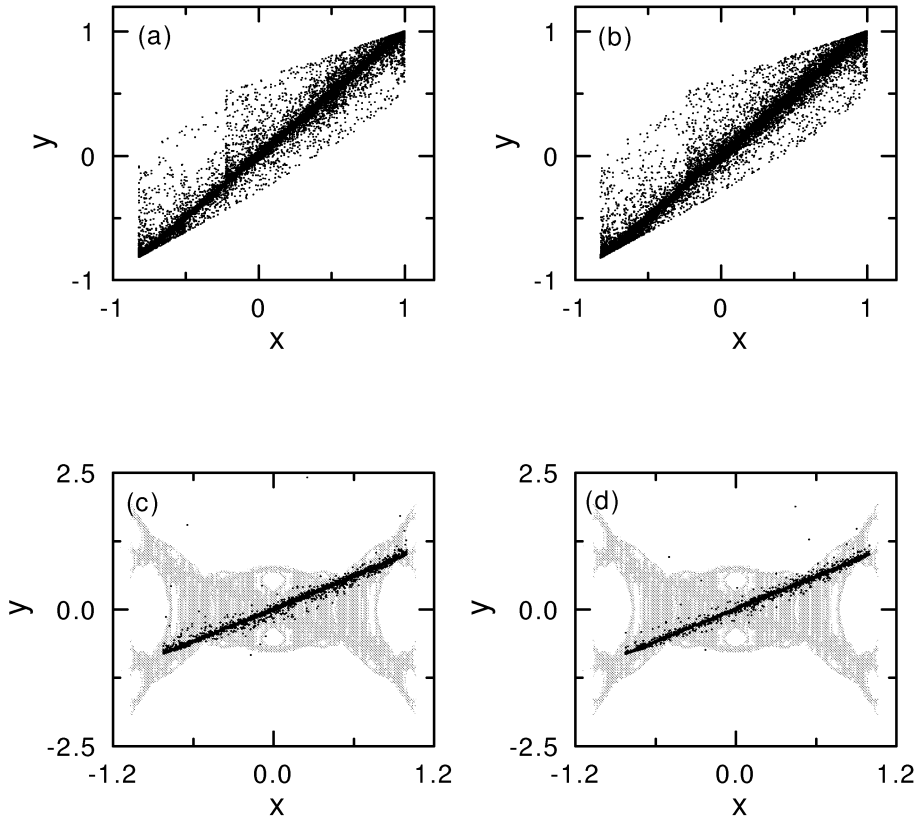

Fig. 1. Effect of parameter mismatch and noise on the weakly stable SCA for $a = 1.82$. The Bubbling attractors for $c = -0.7$ under (a) parameter mismatch with $\varepsilon = 0.001$, and (b) noise with $\delta = 0.0005$. For the riddling case of $c = -2.91$, the weakly stable SCA with a basin (gray region) riddled with a dense set of holes (white region) leading to divergent orbits is transformed into a chaotic transient (black dots) under (c) parameter mismatch with $\varepsilon = 0.001$ and (d) noise with $\delta = 0.0005$.

and riddling transitions occur through the transverse bifurcations of periodic saddles embedded in the SCA, respectively. As a result the SCA becomes weakly stable, because of the local transverse repulsion of periodic repellers embedded in the SCA. In the presence of an absorbing area, however small the parameter mismatching ε and the noise strength δ, a persistent intermittent bursting, called 'attractor bubbling', occurs in the regime of bubbling ($c_{t,r} < c < c_{b,r}$), as shown in Figs. 1(a) and (b). By contrast, in the regime of riddling ($c_{b,l} < c < c_{t,l}$), the weakly stable SCA with a riddled basin is transformed into a chaotic transient with a finite lifetime [see Figs. 1(c) and 1(d)], because no absorbing area, confining the local bursting, exists. In both the bubbling and riddling cases, the quantity of interest is the average time τ that a typical trajectory spends near the diagonal (i.e., the average interburst interval of the bubbling attractor and the average lifetime of the chaotic transient). Therefore, we investigate how τ scales with the mismatching parameter ε and the noise strength δ.

We first consider the case of attractor bubbling. As c passes through $c_{t,r}$, a

bubbling transition occurs through the first transverse supercritical period-doubling bifurcation of the saddle fixed point embedded in the SCA.[11] For this case, the bursting from the diagonal can be represented by the transverse variable

$$u_n = x_n - y_n, \tag{4}$$

denoting the deviation from synchronization. Then, the bubbling attractor is in the laminar phase when the magnitude of the deviation from the diagonal is less than a threshold value u_b^* (i.e., $|u_n| < u_b^*$). Otherwise, it is in the bursting phase. Here u_b^* is very small compared to the maximum bursting amplitude $u_{\max}^*$ (i.e., $u_b^* << u_{\max}^*$).

For a given c, we decrease the mismatching parameter ε or the noise strength δ and compute the average laminar length τ_b (i.e., the average interburst interval). For each value of ε or δ, we choose the threshold value as $u_b^* = 0.001$, and follow the trajectory starting from the initial point (0,0) until 50,000 laminar phases are obtained. In this way, we obtain τ_b that scales with ε or δ as follows. It is shown theoretically in Refs. 7) and 18) that just past $c_{t,r}$, τ_b scales with ε or δ or

$$\tau_b \sim e^{\eta_p \varepsilon^{-\alpha_p}} \quad \text{or} \quad \tau_b \sim e^{\eta_n \delta^{-\alpha_n}}. \tag{5}$$

Note that the scaling exponent α depends on the leading term of the evolution equation of the bursting variable u_n. Since the leading nonlinear term for the case of the period-doubling bifurcation is cubic, the scaling exponents α_p and α_n become 2/3, and the scaling constants η_p and η_n are positive constants to be fitted. Figures 2(a) and (b) display the plots of $\log_{10}\langle\tau_b\rangle$ versus $\varepsilon^{-2/3}$ and $\delta^{-2/3}$ for $c = -0.82$, respectively. Note that these plots are fit well by lines, which implies that Eq. (5) is obeyed to good accuracy. As ε or δ decreases, the average interburst interval τ_b increases faster than any power of ε^{-1} or δ^{-1}. In this way, we see that near $c = c_{t,r}$, τ_b exhibits a "superpower-law" scaling, and hence it becomes extremely long.

However, as c is increased further, a transition from superpower-law to power-law scaling occurs when passing the crossover region $-0.79 \lesssim c \lesssim -0.78$. Thus, for $c \gtrsim -0.78$, the average interburst interval τ_b scales with ε or δ as

$$\tau_b \sim \varepsilon^{-\mu_p} \quad \text{or} \quad \tau_b \sim \delta^{-\mu_n}, \tag{6}$$

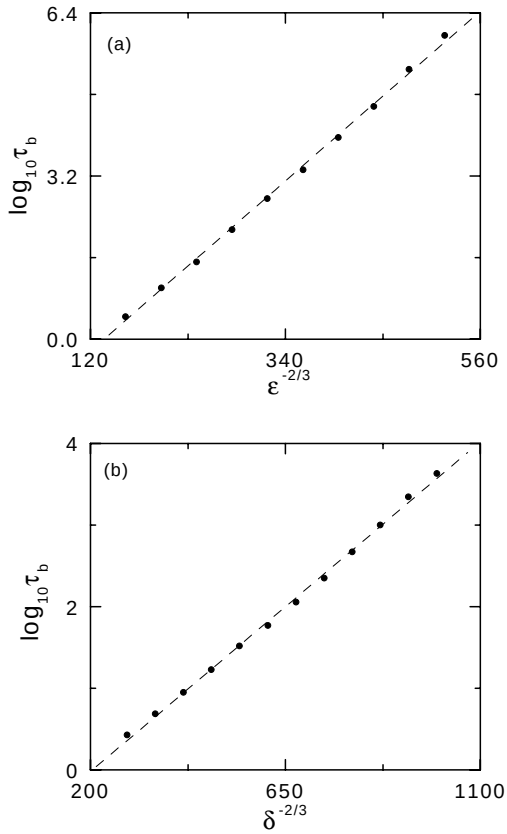

Fig. 2. Plots of $\log_{10}\tau_b$ versus (a) $\varepsilon^{-2/3}$ and (b) $\delta^{-2/3}$ for $c = -0.82$. The average interburst interval τ_b obeys a "superpower-law" scaling. The fitted slopes in (a) and (b) are $\eta_p = 0.036$ and $\eta_n = 0.0049$, respectively.

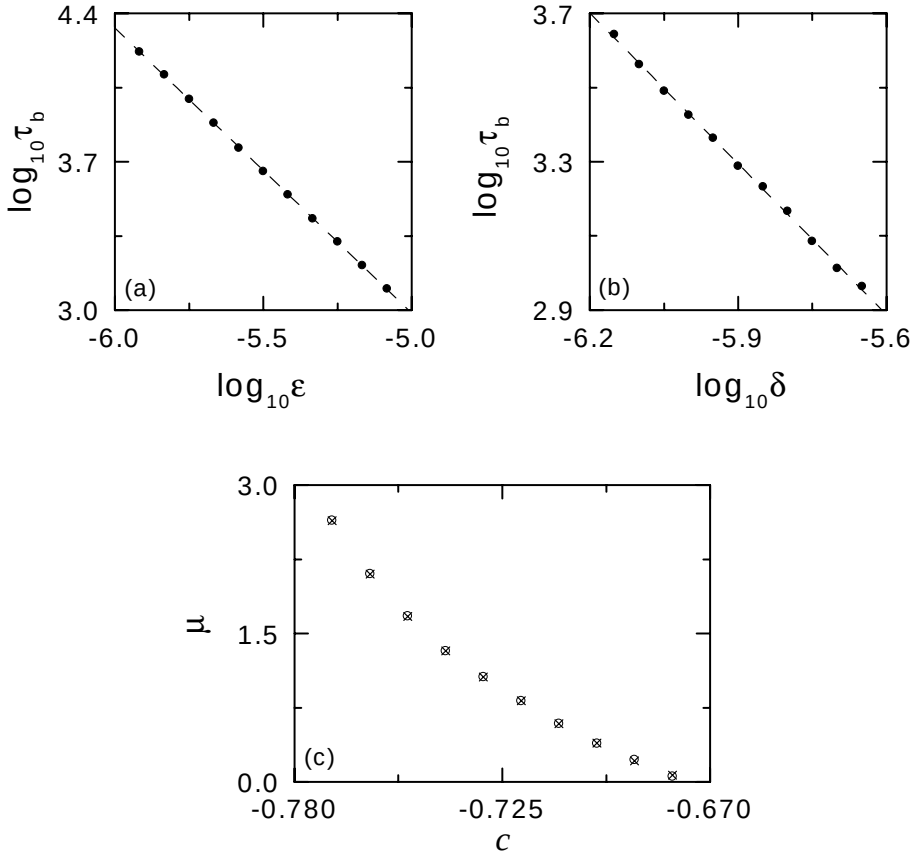

Fig. 3. Plots of $\log_{10}\tau_b$ versus (a) $\log_{10}\varepsilon$ and (b) $\log_{10}\delta$ for $c = -0.74$. For both cases, the average interburst interval obeys a power-law scaling, with the same exponent $\mu \simeq 1.32$. The plot of the scaling exponents μ_p (open circles) and μ_n (crosses) versus c for the case of parameter mismatch and noise is displayed in (c).

where μ_p and μ_n are the scaling exponents for the cases of parameter mismatch and noise, respectively. Figures 3(a) and (b) display the plots of $\log_{10}\langle\tau_b\rangle$ versus $\log_{10}\varepsilon$ and $\log_{10}\delta$ for $c = -0.74$, respectively. These plots are fit well by lines, and hence we find that Eq. (6) obeyed with good accuracy. For this case the slopes of the fitted lines give the values of the exponents μ_p and μ_n. Note that the values of μ_p ($\simeq 1.32$) and μ_n ($\simeq 1.32$) become the same within numerical accuracy. In this way, by varying the coupling parameter from $c = -0.77$ to $c = -0.68$, we obtain the scaling exponents μ_p and μ_n. They are plotted in Fig. 3(c). Note that the values of μ_p (denoted by the circles) agree well with those of μ_n. Thus, the scaling results for the cases of parameter mismatch and noise become the same (within numerical accuracy). As c increases toward the blow-out bifurcation point $c_{b,r}$, the value of the exponent μ becomes smaller, and hence the average interburst interval becomes shorter.

We next consider the case of chaotic transients. As c passes through $c_{t,l}$, a riddling transition occurs through a transcritical contact bifurcation of the saddle

fixed point embedded in the SCA.[11] After that, the SCA with a riddled basin is transformed into a chaotic transient with a finite lifetime, because there exists no absorbing area confining the local bursting. For a given value of c, we decrease the mismatching parameter ε or the noise strength δ and compute the average lifetime τ_c as follows. For each value of ε or δ, we consider an ensemble of trajectories starting from 1000 initial points chosen randomly with uniform probability in the range of $x \in (1-a, 1)$ on the diagonal $y = x$. A trajectory may be regarded as having escaped once the magnitude of its y value becomes larger than 10, because an orbit with $|y| > 10$ lies sufficiently outside the basin of the SCA. Thus we obtain a τ_c that scales with ε or δ as follows. Just past $c_{t,l}$, τ_c exhibits a superpower-law scaling with respect to the variation of ε or δ,

$$\tau_c \sim e^{\zeta_p \varepsilon^{-\beta_p}} \quad \text{or} \quad \tau_c \sim e^{\zeta_n \delta^{-\beta_n}}, \tag{7}$$

as shown in Figs. 4(a) and (b) for $c = -2.795$. Note that, in the case of a transcritical bifurcation, the leading nonlinear term for the evolution equation of u_n becomes quadratic, in contrast to the bubbling case, in which there is a leading cubic term. Hence, for both the cases of parameter and noise, the scaling exponents β_p and β_n become $1/2$,[7),18),11)] in contrast to the bubbling case, with the scaling exponents $\alpha_p = \alpha_n = 2/3$, and the scaling constants ζ_p and ζ_n are positive constants to be fitted. Consequently, near $c = c_{t,l}$, τ_c increases faster than any power of ε^{-1} or δ^{-1} as ε or δ decreases to zero, and hence the chaotic transient becomes extremely long-lived.

However, as c is decreased further, a transition from the superpower-law to a power-law scaling occurs when passing the crossover region $-2.84 \lesssim c \lesssim -2.81$. Thus, for $c \lesssim -2.84$, the average lifetime τ_c scales with ε or δ as

$$\tau_c \sim \varepsilon^{-\nu_p} \quad \text{or} \quad \tau_c \sim \delta^{-\nu_n}, \tag{8}$$

where ν_p and ν_n are the scaling exponents for the cases of parameter mismatch and noise, respectively. When plotting $\log_{10}\tau_c$ versus $\log_{10}\varepsilon$ or $\log_{10}\delta$, the slope gives the scaling exponent ν_p or ν_n. Figure 4(c) displays the plots of ν_p (denoted by circles) and ν_n (denoted by crosses) versus c for $-2.95 \le c \le -2.85$. Note that the values of ν_p agree well with those of ν_n. As in the case of attractor bubbling, the scaling results for the cases of parameter mismatch and noise become the same (within numerical accuracy). As c increases toward the blow-out bifurcation point $c_{b,l}$, the value of the exponent ν becomes smaller, and hence the average lifetime becomes shorter.

Finally, we explain the theoretical background of the power-law behavior by comparing our numerical result with a theoretical result. Consider a parallel line with a distance d from the diagonal as characterizing the measure of the basin riddling in absence of parameter mismatch and noise. For a given c, we choose 2,000 randomly chosen initial conditions on the $y = x + d$ line, and determine in which basin they lie. Then, the "divergence probability" $P(d)$ is estimated as the fraction of the points that are attracted to infinity. It was numerically found that $P(d)$ scales with d as[11]

$$P(d) \sim d^{\gamma}, \tag{9}$$

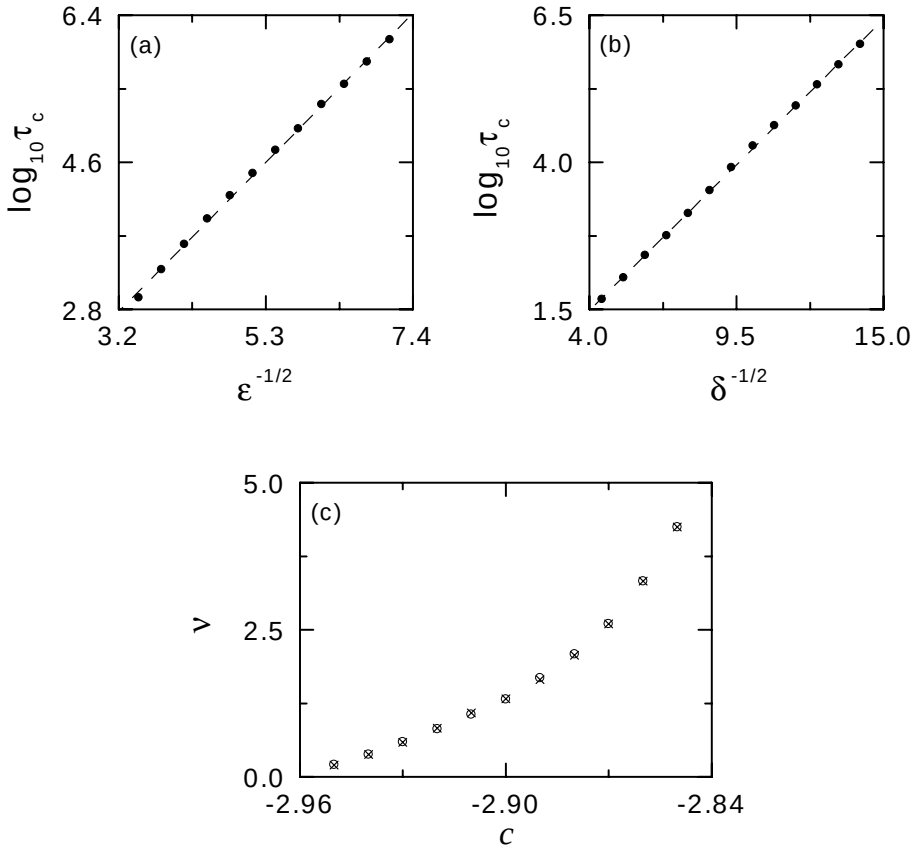

Fig. 4. Plots of $\log_{10}\tau_c$ versus (a) $\varepsilon^{-1/2}$ and (b) $\delta^{-1/2}$ for $c = -2.795$. The average lifetime τ_c of the chaotic transient obeys a "superpower-law" scaling. The fitted slopes in (a) and (b) are $\zeta_p = 1.944$ and $\zeta_n = 0.435$, respectively. After passing a crossover region, τ_c exhibits a power-law scaling. The plot of the scaling exponents ν_p (open circles) and ν_n (crosses) versus c for the cases of parameter mismatch and noise are displayed in (c).

where γ is referred to as the 'divergence exponent'. Figure 5(a) displays plot of γ (denoted by pluses) versus c. As c decreases toward the blow-out bifurcation point $c_{b,l}$, the value of γ becomes smaller, and hence the measure of the basin riddling increases. However, in presence of any small parameter mismatch or noise, the SCA on the diagonal is transformed into a chaotic transient with a finite lifetime τ_c, as shown in Figs. 1(c) and (d). As explained above, τ_c is obtained by averaging the estimated lifetime of the chaotic transients, starting from randomly chosen initial conditions on the diagonal. One can easily imagine that τ_c is in reciprocal proportion to the divergence probablity $P(d)$ and that the distance d from the diagonal is in proportion to ϵ or δ. With such relations, the exponent ν (denoted by the open circles) for the average lifetime of the chaotic transient becomes nearly the same as the divergence exponent (denoted by pluses) γ, as shown in Fig. 5(a). In Ref. 19), Ott et al. introduced a random walk model for the evolution of the bursting variable u_n and, using the diffusion approximation, they found that the divergence exponent

γ is given by

$$\gamma = \frac{|\sigma_T|}{D}. \qquad (10)$$

Here σ_T is the (average) transverse Lyapunov exponent, and D is a quantity characterizing the decrease with increasing time of the dispersion of local (M-time) transverse Lyapunov exponent σ_M^T [i.e., $\langle(\sigma_M^T - \langle\sigma_M^T\rangle)^2\rangle$], where $\langle\cdots\rangle$ denotes the average over an ensemble of initial conditions. Such a dispersion approaches zero in a form inversely proportional to M as follows:

$$\langle(\sigma_M^T - \langle\sigma_M^T\rangle)^2\rangle = \frac{2D}{M}. \qquad (11)$$

Here the value of D ($\simeq 0.054$) is the same for all values of c for $a = 1.82$ in the regime of weak synchronization. [20] Furthermore, Eq. (10) is valid only near the blow-out bifurcation point (i.e., in the region where the value of σ_T becomes very small). [19] The solid line in Fig. 5 has slope given by Eq. (10), with numerically obtained σ_T and D. Note that the numerical and theoretical results agree well near the blow-out bifurcation point $c_{b,l}$. However, as c increases toward the riddling transition point, the theoretical result deviates from the numerical result. Furthermore, we conjecture that the scaling exponent μ for the average interburst interval of the bubbling attractor may be given by the same Eq. (10), because both the chaotic transient and attractor bubbling exist, due to the existence of positive local transverse Lyapunov exponents for the weakly stable SCA. We note that the solid line with slope given by Eq. (10) also agrees well with the scaling exponent μ only near the blow-out bifurcation point $c_{b,r}$. Hence, more rigorous theoretical analysis may be required to explain the numerical data for the scaling exponents μ and ν near the bubbling and riddling transition points.

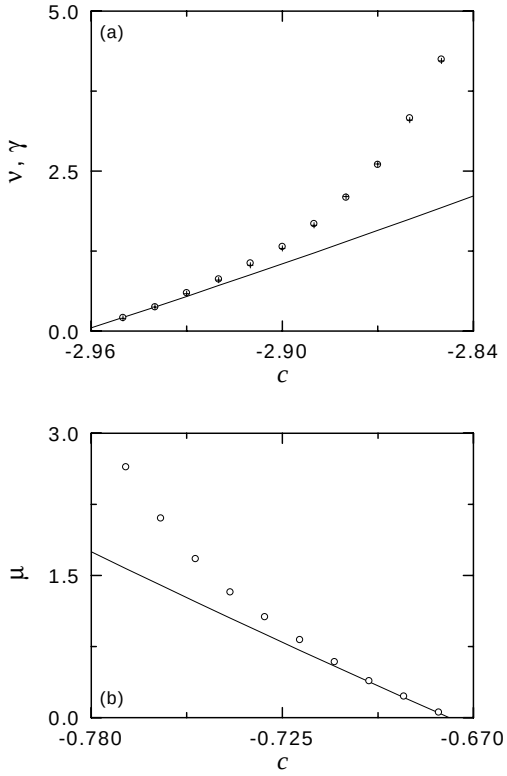

Fig. 5. (a) Plots of the divergence exponents γ (denoted by pluses) and the scaling exponents ν (denoted by open circles) for the chaotic transients, in the presence of the parameter mismatch, versus c. Note that the values of the exponents γ and ν become nearly the same. The solid line has a slope given by Eq. (10). Near the left blow-out bifurcation point $c_{b,l}$, this theoretical result agrees well with the numerical result. (b) Plots of the scaling exponents μ (denoted by the open circles) for the attractor bubbling, in presence of the parameter mismatch, versus c. The solid line with a slope given by Eq. (10) agrees well with the numerical result near the right blow-out bifurcation point $c_{b,r}$.

§3. Maximum bursting amplitude for attractor bubbling

In this section we investigate the change in the maximum bursting amplitude for attractor bubbling by increasing the coupling parameter from the bubbling transition point $c_{t,r}$ ($= -0.850\,625$). When passing through $c_{t,r}$, the saddle fixed point embedded in the SCA first becomes transversely unstable via a transverse supercritical period-doubling bifurcation giving rise to the birth of an asynchronous period-2 saddle. As a result, the SCA becomes weakly stable, because trajectories visiting neighborhoods of the repelling fixed point and its preimages on the diagonal are locally repelled. However, these locally repelled trajectories are confined to move within the mixed absorbing area, whose boundary is formed by the union of segments of the critical curves L_k ($k = 1, 2$) and portions of unstable manifolds of the newly-born asynchronous period-2 saddle. Then, the maximum bursting amplitude $d_{\max}$ ($= |y - x|_{\max}$) from the diagonal is determined by the maximum vertical size, $|y - x|_{\max}$, of such a mixed absorbing area.

As an example, we consider the bubbling attractor for $a = 1.82$. Figures 6(a)

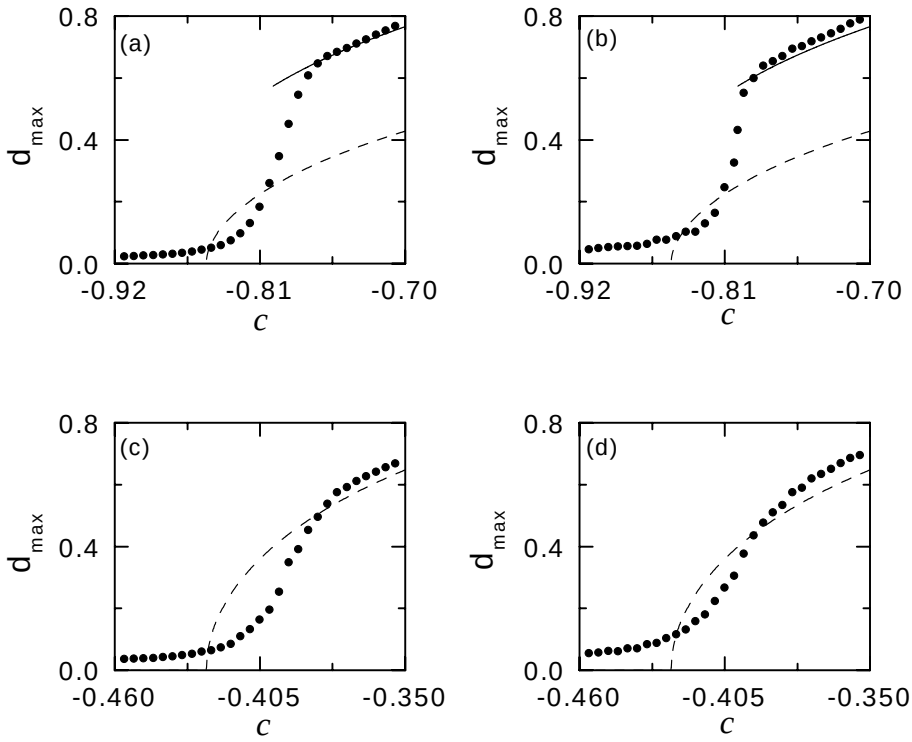

Fig. 6. Plots of $d_{\max}$ versus c for $a = 1.82$ in the unidirectionally coupled case for (a) $\varepsilon = 0.006$ and (b) $\delta = 0.002$. The values of $d_{\max}$ are denoted by the solid circles. The dashed and solid lines represent the maximum values of $|y - x|$ for the asynchronous period-2 and period-3 saddles, respectively, for $\varepsilon = \delta = 0$. Plots of $d_{\max}$ versus c for $a = 1.82$ in the symmetrically coupled case for (c) $\varepsilon = 0.01$ and (d) $\delta = 0.004$. The values of $d_{\max}$ are denoted by the solid circles, and the dashed line represents the maximum values of $|y - x|$ for the asynchronous period-2 saddle with $\varepsilon = \delta = 0$.

and (b) display the plot of $d_{\max}$ versus c for the mismatching parameter $\varepsilon = 0.006$ and the noise strength $\delta = 0.002$, respectively. Here the value of $d_{\max}$ is obtained by following the trajectory starting from the initial point $(0.5, 0.5)$ up to the time $n = 10^8$. When passing $c_{t,r}$, $d_{\max}$ (denoted by the solid circles) begins to increase smoothly, because of the transverse repulsion of the repelling fixed point on the diagonal. However, since the "strength" of this transverse repulsion is very weak near $c = c_{t,r}$, the iteration number $n = 10^8$ is not sufficient for the trajectory to approach the vicinity of the asynchronous period-2 saddle on the boundary of the mixed absorbing area, whose maximum distance, $|y - x|_{\max}$, from the diagonal for $\varepsilon = \delta = 0$ is denoted by the dashed line. Hence, the numerically obtained values of $d_{\max}$ lie below the dashed line near $c = c_{t,r}$. However, as c is increased further, the mixed absorbing area becomes broken up through a collision with a periodic repeller, and then a new larger absorbing area bounded by the union of segments of unstable manifolds of the asynchronous period-3 saddle and portions of the critical curves L_1 and L_2 confines the bursting. (A detailed explanation of the abrupt increase in the absorbing area via an interior crisis is given below.) Thus the maximum bursting amplitude abruptly increases up to the maximum value of $|y - x|$ for the asynchronous period-3 saddle (denoted by the solid lines), as shown in Figs. 6(a) and (b). However, this kind of abrupt increase in $d_{\max}$ does not occur in symmetrically coupled 1D maps, given by

$$T : \begin{cases} x_{n+1} = f(x_n, a) + c\, g(x_n, y_n) + \delta\, \xi_n^{(1)}, \\ y_{n+1} = f(y_n, b) + c\, g(y_n, x_n) + \delta\, \xi_n^{(2)}, \end{cases} \tag{12}$$

where $b = a - \varepsilon$ and $g(x, y) = y^2 - x^2$. The mixed absorbing area whose boundary is formed by portions of unstable manifolds of the asynchronous period-2 saddle and segments of the critical curves L_1 and L_2 persists under the change of c, in contrast to the above studied unidirectionally coupled case. Hence, as c is increased from the bubbling transition point $c_{t,r}$ $(= -0.425\,313)$, $d_{\max}$ increases smoothly up to the maximum value of $|y - x|$ for the asynchronous period-2 saddle (denoted by the dashed lines), as shown in Figs. 6(c) and (d).

Finally, we discuss the interior crisis of the mixed absorbing area occurring for the case $\varepsilon = \delta = 0$, which causes an abrupt increase in the maximum bursting amplitude. Figure 7(a) depicts two mixed absorbing areas surrounding the SCA on the diagonal for $c = -0.85$. The segments of unstable manifolds (whose directions are denoted by arrows) of the asynchronous period-2 saddle (denoted by the crosses) connect to the segments of the critical curves L_1 and L_2 (the dots denote where the segments connect), and defines a mixed absorbing area. Here an asynchronous period-2 saddle is born from the synchronous fixed point (denoted by the star) via a transverse supercritical period-doubling bifurcation and moves away from the diagonal. Locally repelled trajectories are then confined to move within this minimal absorbing area, shaded gray. The boundary of the outer mixed absorbing area is formed by the union of segments of unstable manifolds of the asynchronous period-3 saddle (denoted by the open circles) and portions of the critical curves L_1 and L_2. For this case, the period-3 saddle emerges together with another period-3 repeller (denoted by the solid

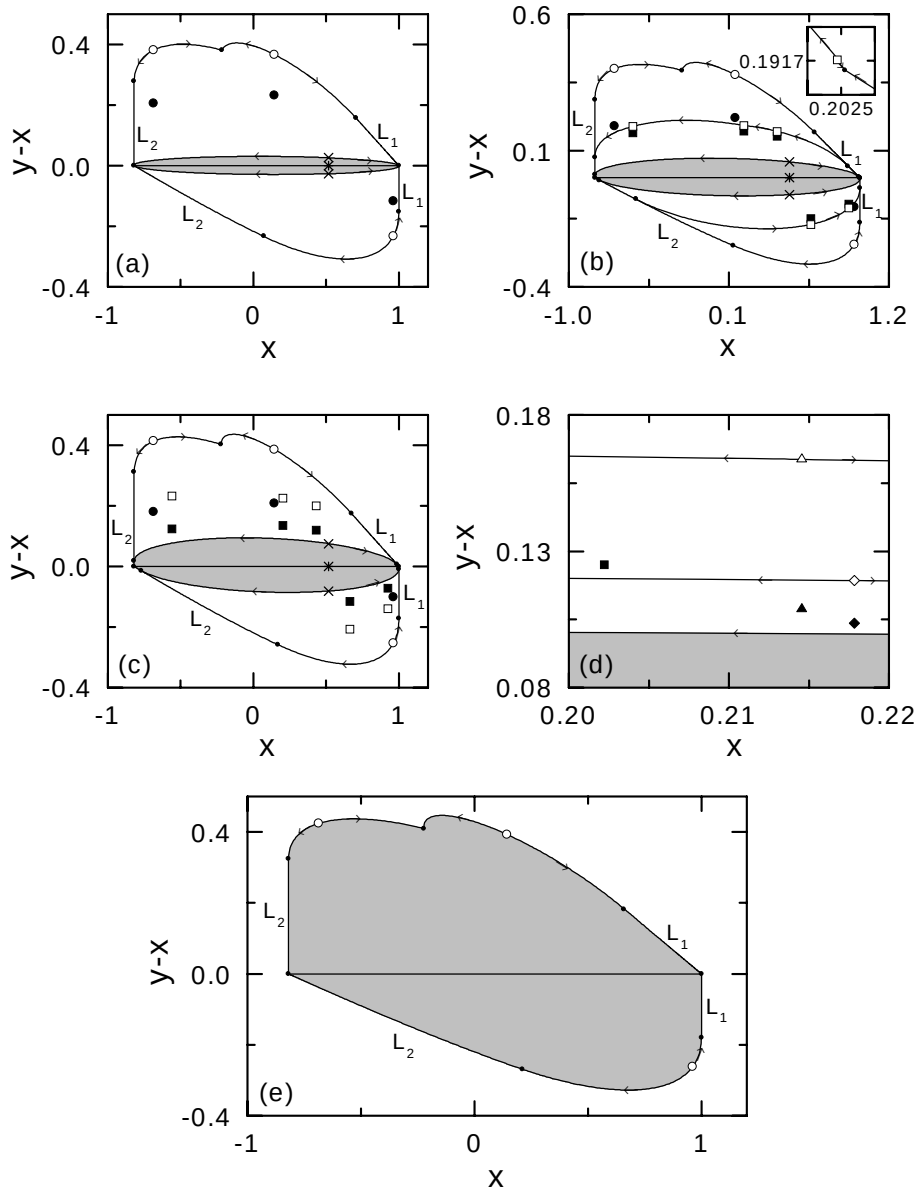

Fig. 7. Sudden increase in the absorbing area via an interior crisis for $a = 1.82$. Absorbing areas for $c = -0.85$, -0.8473, -0.845, -0.84375, and -0.843 are shown in (a), (b), (c), (d), and (e), respectivey. Here, the minimal absorbing areas confining the local bursting are shaded gray. The minimal absorbing area in (a) is bounded by the union of portions of unstable manifolds of the asynchronous period-2 saddle (denoted by the crosses) that is born from the synchronous fixed point (denoted by the star) through a transverse supercritical period-doubling bifurcation and segments of the critical curves L_1 and L_2. This small minimal absorbing area becomes broken up through a collision with a period-9 repeller (denoted by the solid diamond), and then a larger minimal absorbing area appears, as shown in (e). The period-3, 5, 7, and 9 saddles and repellers are denoted by open and solid circles, squares, triangles, and diamonds, respectively. The arrows denote the directions of unstable manifolds of periodic saddles, and the dots represent where the segments of unstable manifolds and critical curves L_1 and L_2 connect. (For more details, see the text.)

circles) via a saddle-node bifurcation for $c \simeq -0.8565$. As c is increased further, successive saddle-node bifurcations giving rise to the birth of higher period, $q = 5, 7$, and 9, saddles and repellers also occur inside the outer mixed absorbing area for $c \simeq -0.8474$, -0.8445, and -0.8437, respectively. For this case, all the repellers move toward the diagonal, while all the saddles move far away from the diagonal. Figure 7(b) shows that between the outermost and innermost absorbing areas, a new absorbing area is bounded by the union of portions of unstable manifolds of the period-5 saddles (denoted by the open squares) and segments of the critical curves L_1 and L_2. However, as c is increased further, the period-3 repeller (denoted by the solid circles) approaches and penetrates this new absorbing area for $c \simeq -0.8465$. Then, due to this crisis, the intermediate absorbing area becomes broken up, as shown in Fig. 7(c) for $c = -0.845$. Unlike this period-5 case, unstable manifolds of the period-7 (denoted by the open triangles) and period-9 (denoted by the open diamonds) saddles cannot bound any mixed absorbing areas, because there already exist period-5 (denoted by the solid squares) and period-7 (denoted by the solid triangles) repellers below the unstable manifolds of the period-7 and period-9 saddles, respectively, as shown in Fig. 7(d) for $c = -0.84375$. Eventually, the period-9 repeller (denoted by the solid diamond) penetrates into the minial absorbing area and breaks it up for $c = -0.8437$. Then, the outmost absorbing area becomes a new minimal absorbing area, as shown in Fig. 7(e). Due to this kind of the interior crisis, an abrupt increase in the minimal absorbing area occurs. Consequently, the maximum bursting amplitude also increases suddenly, up to the maximum value of $|y - x|$ for the period-3 saddle, denoted by the solid lines in Figs. 6(a) and (b).

§4. Summary

We have numerically studied the effect of parameter mismatch and noise on the bubbling and basin riddling. No matter how small the parameter mismatch or noise, the weakly stable SCA is transformed into a bubbling attractor or a chaotic transient, depending on the existence of an absorbing area controlling the global dynamics. We first investigated how the average interburst interval of the bubbling attractor and the average lifetime of the chaotic transient scale with mismatch parameter ε and the noise intensity δ. Just past the first transverse bifurcation point, such an average time τ exhibits a "superpower-law" scaling that increases faster than any power-law as ε and δ tend to zero. However, after passing a crossover region, τ exhibits a power-law scaling. Moreover, the scaling exponents for the cases of parameter mismatch and noise are the same. We have also given the theoretical background for the scaling by comparing our numerical results with theoretical results. We next investigated the maximum bursting amplitude for the case of attractor bubbling. When passing a threshold value, the maximum bursting amplitude has been found to increase abruptly via the interior crisis of an absorbing area, in contrast to the symmetric-coupling case, in which such an interior crisis of the absorbing area does not occur.

Acknowledgements

This work was supported by the Korea Research Foundation under Grant No. KRF-2001-015-DP0075.

References

1) H. Fujisaka and T. Yamada, Prog. Theor. Phys. **69** (1983), 32.
2) A. S. Pikovsky, Z. Phys. B **50** (1984), 149.
3) V. S. Afraimovich, N. N. Verichev and M. I. Rabinovich, Radiophys. Quantum Electron. **29** (1986), 795.
4) L. M. Pecora and T. L. Carroll, Phys. Rev. Lett. **64** (1990), 821.
5) K. M. Cuomo and A. V. Oppenheim, Phys. Rev. Lett. **71** (1993), 65.
L. Kocarev, K. S. Halle, K. Eckert, L. O. Chua and U. Parlitz, Int. J. Bifurcation Chaos Appl. Sci. Eng. **2** (1992), 973.
L. Kocarev and U. Parlitz, Phys. Rev. Lett. **74** (1995), 5028.
N. F. Rulkov, Chaos **6** (1996), 262.
6) P. Ashwin, J. Buescu and I. Stewart, Nonlinearity **9** (1996), 703.
7) Y.-C. Lai, C. Grebogi, J. A. Yorke and S. C. Venkataramani, Phys. Rev. Lett. **77** (1996), 55.
8) V. Astakhov, A. Shabunin, T. Kapitaniak and V. Anishchenko, Phys. Rev. Lett. **79** (1997), 1014.
9) Yu. L. Maistrenko, V. L. Maistrenko, A. Popovich and E. Mosekilde, Phys. Rev. E **57** (1998), 2713; ibid. **60** (1999), 2817.
O. Popovych, Yu. L. Maistrenko, E. Moskilde, A. Pikovsky and J. Kurths, Phys. Lett. A **275** (2000), 401; Phys. Rev. E **63** (2001), 036201.
10) Yu. L. Maistrenko, V. L. Maistrenko, A. Popovich and E. Mosekilde, Phys. Rev. Lett. **80** (1998), 1638.
G.-I. Bischi and L. Gardini, Phys. Rev. E **58** (1998), 5710.
11) S.-Y. Kim and W. Lim, Phys. Rev. E **63** (2001), 026217.
S.-Y. Kim, W. Lim and Y. Kim, Prog. Theor. Phys. **105** (2001), 187.
12) S.-Y. Kim and W. Lim, Phys. Rev. E **64** (2001), 016211.
13) C. Mira, L. Gardini, A. Barugola and J.-C. Cathala, *Chaotic Dynamics in Two-Dimensional Noninvertible Maps* (World Scientific, Singapore, 1996).
R. H. Abraham, L. Gardini and C. Mira, *Chaos in Discrete Dynamical Systems* (Springer, New York, 1997).
14) P. Ashwin, J. Buescu and I. Stewart, Phys. Lett. A **193** (1994), 126.
J. F. Heagy, T. L. Carroll and L. M. Pecora, Phys. Rev. E **52** (1995), 1253.
S. C. Venkataramani, B. R. Hunt, E. Ott, D. J. Gauthier and J. C. Bienfang, Phys. Rev. Lett. **77** (1996), 5361.
15) S. C. Venkataramani, B. R. Hunt and E. Ott, Phys. Rev. E **54** (1996), 1346.
16) J. C. Alexander, J. A. Yorke, Z. You and I. Kan, Int. J. Bifurcation Chaos Appl. Sci. Eng. **2** (1992), 795.
E. Ott, J. C. Sommerer, J. C. Alexander, I. Kan and J. A. Yorke, Phys. Rev. Lett. **71** (1993), 4134.
J. C. Sommerer and E. Ott, Nature (London) **365** (1993), 136.
E. Ott, J. C. Alexander, I. Kan, J. C. Sommerer and J. A. Yorke, Physica D **76** (1994), 384.
J. F. Heagy, T. L. Carroll and L. M. Pecora, Phys. Rev. Lett. **73** (1994), 3528.
17) E. Ott and J. C. Sommerer, Phys. Lett. A **188** (1994), 39.
Y. Nagai and Y.-C. Lai, Phys. Rev. E **56** (1997), 4031.
18) C. Grebogi, E. Ott and J. A. Yorke, Phys. Rev. Lett. **50** (1983), 935; Erg. Th. Dyna. Sys. **5** (1985), 341.
19) E. Ott, J. C. Sommerer, J. C. Alexander, I. Kan and J. A. Yorke, Phys. Rev. Lett. **71** (1993), 4134.
E. Ott, J. C. Alexander, I. Kan, J. C. Sommerer and J. A. Yorke, Physica D **76** (1994), 384.
20) A. Jalnine and S.-Y. Kim, Phys. Rev. E **65** (2002), 026210.